Applications of advanced transmission electron microscopic techniques to Ni–Ti based shape memory materials

Dominique Schryvers*, Pavel Potapov, Rubén Santamarta[1], Wim Tirry

Electron Microscopy for Materials Research (EMAT), University of Antwerp (RUCA), Groenenborgerlaan 171, B-2020 Antwerp, Belgium

Abstract

In the present contribution some recent results of advanced transmission electron microscopy applications on Ni–Ti based shape memory materials will be reviewed. These will include the precipitate growth in binary $Ni_{51}Ti_{49}$ in which lens-shaped Ni_4Ti_3 precipitates are grown and which induce particular strain fields in the surrounding matrix influencing any ensuing martensitic transformation. Special image treatment methods are used to measure the actual lattice deformations close to these precipitates. Also the crystallisation process occurring in $Ti_{50}Ni_{25}Cu_{25}$ melt-spun ribbons is investigated in which the focus is on the domain, interface and surface structure of micron-sized spherical B2 particles growing inside the amorphous material. When particles grow larger, martensite plates as well as small planer defects are observed.
© 2004 Elsevier B.V. All rights reserved.

Keywords: Ni–Ti; HRTEM; Precipitation; Crystallisation

1. Introduction

The evolution of modern transmission electron microscopes (TEM) to more integrated instruments allows for the simultaneous investigation of different aspects of a material while retaining most of the extremely high resolution and precision of dedicated instruments. At the same time advanced imaging capturing techniques and treatments yield a more quantitative interpretation of the obtained data which could eventually lead to materials design instead of a mere description of the occurring micro- and nanostructures.

In superelastic Ni–Ti alloys the effects of precipitates in the austenite matrix on the transformation processes of the latter have been studied before [1–3], but no clear data on the actual lattice deformations in the nanoscale vicinity of the precipitates is available. In order to provide more insight in these complex processes, high resolution TEM (HRTEM) combined with numerical analysis of the imaging data has been performed on Ni_4Ti_3 precipitates and the surrounding B2 matrix and it is shown that the matrix indeed strongly deforms in the neighbourhood of the precipitates.

On the other hand, crystallisation of an amorphous ribbon is governed by different physical processes. Micron-sized spherical-like particles are investigated in amorphous $Ti_{50}Ni_{25}Cu_{25}$ melt-spun ribbons in order to understand the grain and domain formation during growth and phase transformation in such particles [4,5]. Single as well as multi-grain B2 particles of different sizes have been observed while the appearance of martensitic plates is found in particles with a diameter above 4 μm.

2. Results and discussions

2.1. Ni_4Ti_3 precipitates in $Ni_{51}Ti_{49}$

$Ni_{51}Ti_{49}$ rods were heat treated in order to form Ni_4Ti_3 precipitates of different numbers and sizes [6,7]. A typical example of the obtained distribution is seen in Fig. 1a. The precipitates are lens-shaped and stay coherent with the matrix as long as their longest axis remains shorter than 250 nm. The Ni_4Ti_3 unit cell can be considered as being built by $3 \times 3 \times 3$ bcc units with slight contractions of the

* Corresponding author. Tel.: +32-3-2653247; fax: +32-3-2653257.
E-mail addresses: nick.schryvers@ua.ac.be (D. Schryvers),
ruben.santamarta@uib.es (R. Santamarta).
[1] From 1 March 2004 in: Departament de Física, Universitat de les Illes Balears, Cra. de Valldemossa, km. 7.5, E- 07122 Palma de Mallorca, Spain. Fax: +34-971-173426.
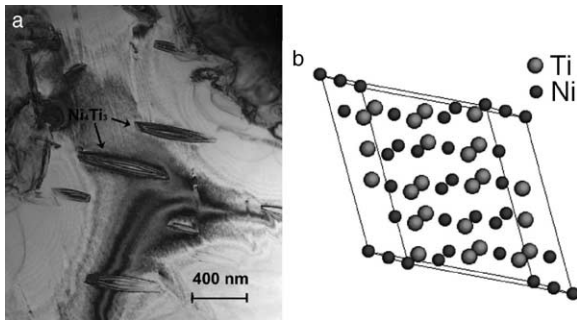
Fig. 1. (a) Typical distribution of the lens-shaped Ni_4Ti_3 precipitates. (b) Hexagonal unit cell.

lattice dimensions resulting in a denser packing [8,9]. However, mostly the hexagonal cell depicted in Fig. 1b is used. These contractions are not isotropic yielding the lens shape with the strongest changes in lattice parameter in the direction perpendicular to the central plane of the lens. In Fig. 2a HRTEM image of two touching Ni_4Ti_3 precipitates observed normal to their central plane (i.e., the c-axis of the hexagonal cell) is shown, together with the corresponding electron diffraction (ED) pattern and simulated HRTEM image, confirming the unit cell suggested by Tadaki et al. [8]. The six-fold supersymmetry is clearly visible. The grain boundary between both precipitates is observed edge-on but does not follow a simple crystallographic plane.

In the directions most strongly affected by the contraction changes up to 3% of interplanar spacing, in the following referred to as %Δd, with respect to the B2 matrix exist. By using HRTEM imaging combined with special image treatment and measuring algorithms, including Fourier transform of lattice resolution images and curve fitting of resulting diffraction spots, these changes can be measured. Any distortions in the digital images were measured on a picture of undistorted material. From this a precision of these measurements of 0.6% Δd is found. An example is shown in Fig. 3 in which the relative change of the $(-101)_{B2}$ interplane spacing is compared with respect to the corresponding set of planes inside the precipitate which are taken as a reference. For this direction, the undistorted austenite matrix has a relative difference with the precipitate spacing of 2.1% which is measured very close to the interface. Further away the differences increase up to 6% at 50 nm with respect to the precipitate spacings, which corresponds to a matrix distortion of around 4%.

Still, the use of calculated reciprocal space data from selected regions from a lattice resolution image implies averaging over several unit cells. In the present case an optimised box size of 5 nm × 5 nm was used for the Fourier transform. More advanced methods like the DALI procedure optimise the contrast of the real space image from which then the position of every white dot can be compared to a reference lattice [10]. For these methods, however, the quality of the original image needs to be very high at every location in the image, whereas the first approach can also work with some diffuse locations as long as these are small compared to the used box. First attempts to apply the DALI procedure seem to indicate that the matrix is strongly expanded in the first few unit cells next to the interface, but that this distortion rapidly decreases over a distance of a few nm, which explains why it is not detected by the first approach which averages over such a small region. Further away from the interface the DALI procedure confirms the earlier results.

2.2. Micron-sized particles in amorphous $Ti_{50}Ni_{25}Cu_{25}$ melt-spun ribbons

Partial crystallisation of amorphous $Ti_{50}Ni_{25}Cu_{25}$ ribbons was performed by selected heat treatments in order to obtain a distribution of individual micron-sized crystalline particles in the amorphous matrix (details on the materials and sample preparation are given in [5]). After thinning to electron transparency, close to all B2 particles show a circular shape indicating that the general three-dimensional shape will be spherical. From this, an isotropic growth can be envisaged, irrespective of the internal microstructure of a given particle. Two typical examples of such particles are presented in Fig. 4a and b, showing a single grain and a multigrain particle, respectively. In both particles a central and more bright circular region of about 100 nm diameter is observed. Selected area ED of a bigger central region (not shown) reveals that this material also has the B2 structure which could indicate local etching by the thinning procedure at an internal defect structure. Energy dispersive X-ray analysis indicates that the particles are homogeneous in composition and
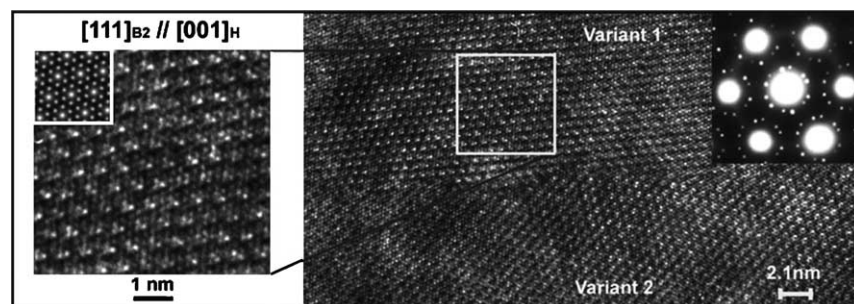

Fig. 2. [0 0 1] HRTEM image and corresponding simulation and ED pattern of a Ni_4Ti_3 precipitate.
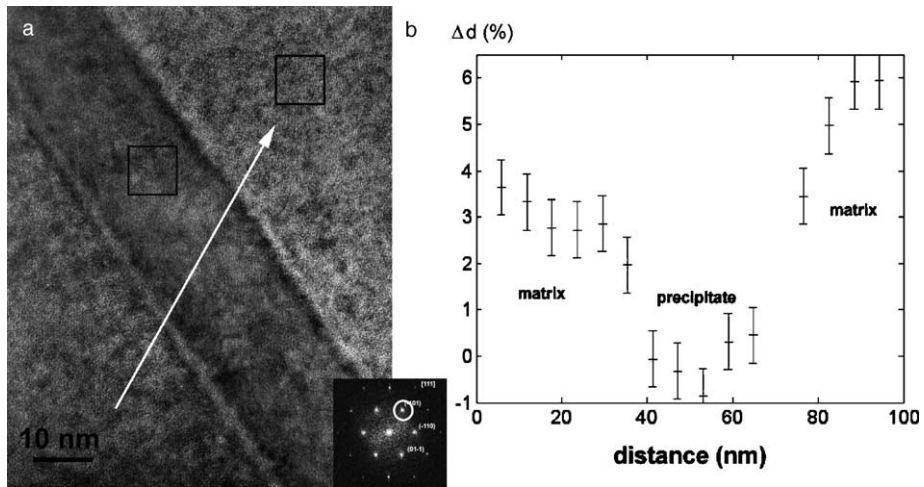
Fig. 3. Measured relative difference for the $(-101)_{B2}$ interplanar distances with respect to the corresponding spacing in the precipitate. Close to the precipitate-matrix interface the matrix is undistorted (2% difference with precipitate reference) whereas the distortion increases at distances further away from the precipitate.
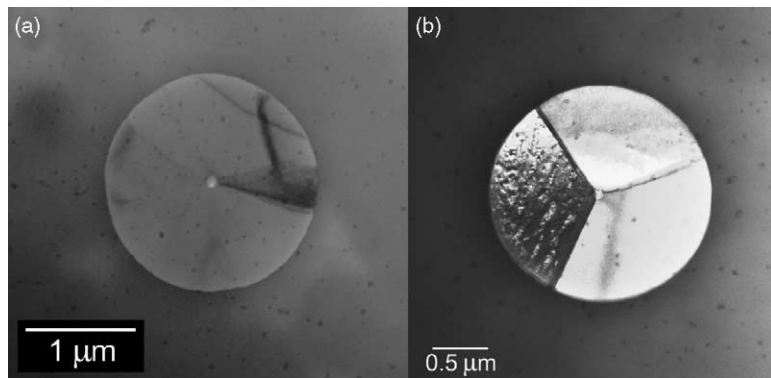

Fig. 4. Micrographs from the $Ti_{50}Ni_{25}Cu_{25}$ ribbon after a thermal treatment of 10 min at 693 K showing two spherical particles with a hole in the centre: (a) single grain and (b) multigrain.
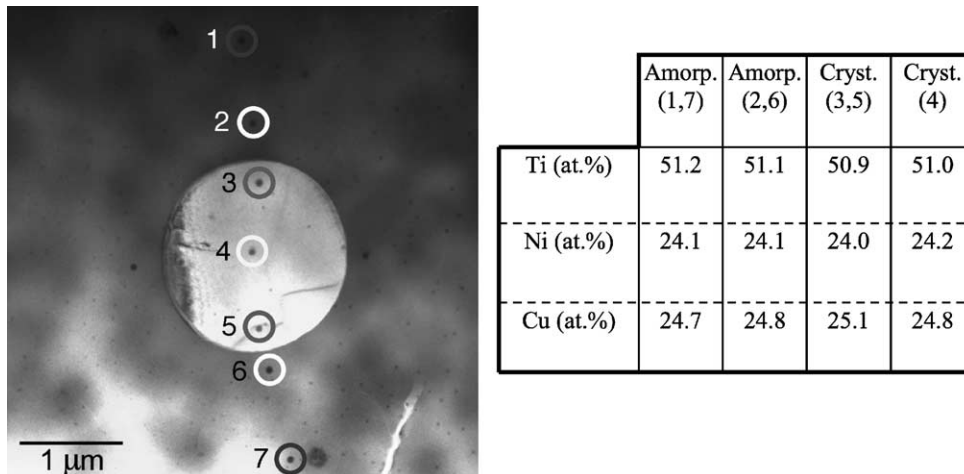

	Amorp. (1,7)	Amorp. (2,6)	Cryst. (3,5)	Cryst. (4)
Ti (at.%)	51.2	51.1	50.9	51.0
Ni (at.%)	24.1	24.1	24.0	24.2
Cu (at.%)	24.7	24.8	25.1	24.8

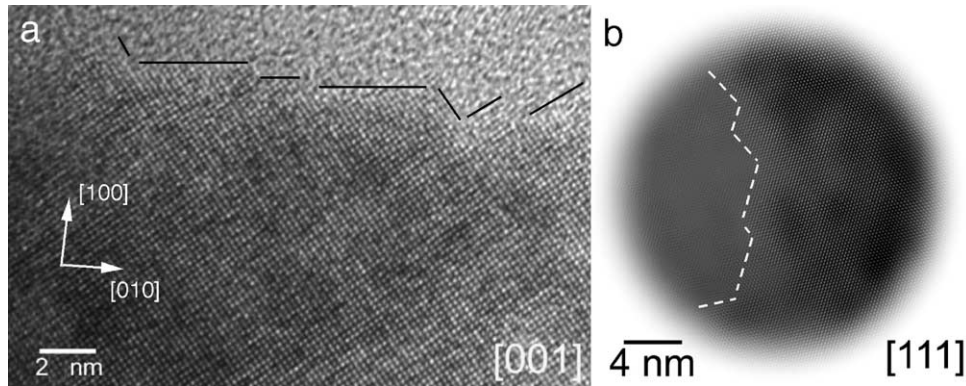Fig. 5. Averaged EDX spot analysis indicating no compositional change during crystallisation.

Fig. 6. (a) [0 0 1] HRTEM image revealing a stepped interface with preference for {1 0 0} and {1 1 0} surface edges for a B2 particle in the amorphous matrix and (b) a Fourier filtered [1 1 1] HRTEM images highlighting the ⟨1 1 0⟩ edges.

retain the chemical ratio's of the amorphous material, as seen in Fig. 5 and the corresponding table listing averaged values obtained from several similar areas.

Although the surface of the particles looks very sharp with a smooth curvature in the images of Fig. 4 a more close observation under HRTEM conditions reveals a more stepped structure. Indeed, in the HRTEM image of Fig. 6a with the particle lattice observed in a [0 0 1] zone the edge of the crystalline area is delineated indicating a preference for {1 0 0} and {1 1 0} surface planes. The same can be observed in other zone orientations such as [1 1 1], e.g. by improving contrast using Fourier filtering as shown in Fig. 6b.

As for the multigrain B2 particles, cases with only two or up to six different grains can be found. Other examples can be found in the contribution by Santamarta and Schryvers [4] where the crystallographic relations between the different grains are further investigated. In most cases typical bcc twinning relations are observed between adjacent grains, although the grain interfaces do not correspond with the cor-responding twin planes. At this stage it seems that most of the two-dimensional images of thinned particles can be explained by a so-called citrus model in which the different grains can be considered as the sections or segments of a citrus fruit and which grow radially from a central common line [11]. Depending on the cut one would see different distributions of these sections.

When the particles are allowed to grown to diameters above 4 μm by a suitable heat treatment [5], multiple-twinned martensite structures are observed. Depending on the particle, the martensite plates are seen to originate from a single or multigrain situation. In Fig. 7 an example of such a particle is shown together with a blow-up of the surface region from another particle. From the latter and the corresponding diffraction patterns it is clear that the martensite twin variants end in a tooth-like configuration and do not completely extend to the edge. Instead, retained austenite exists in between the martensite plates and the surface of the particle.
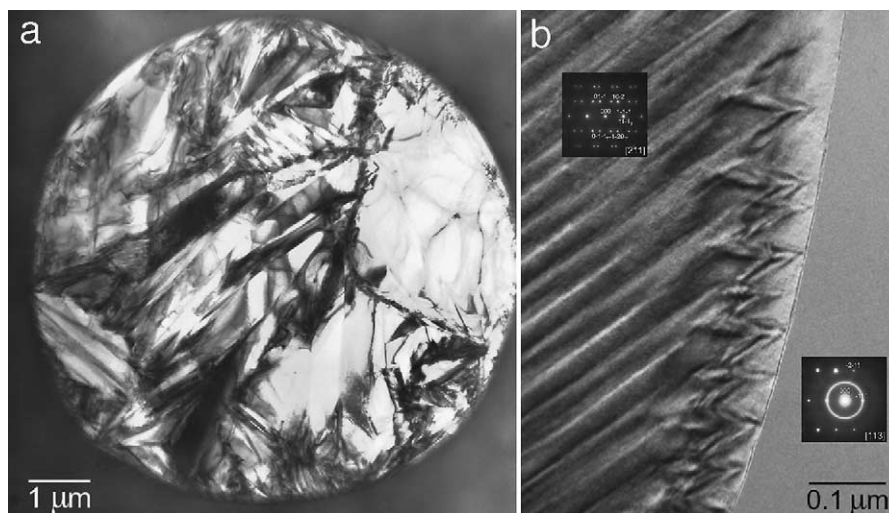

Fig. 7. Micrographs from spherical particles after 10 min at 697 K showing (a) multiple martensite plates and (b) a tooth-like configuration of ending martensite variants with retained austenite (grey areas) at the surface.

3. Conclusions

The present contribution reviews some recent results on precipitation and crystallisation features in Ni–Ti-based shape memory materials. Despite the fact that these systems are already being used for practical applications, still the basic physical processes leading to the relevant microstructures are not completely understood or even described. In the future these results will be complemented by nano-spot elemental analysis for the binary material and more detailed HRTEM and three-dimensional studies on the crystalline particles in the amorphous ribbons.

Acknowledgements

References

[1] L. Bataillard, J.-E. Bidaux, R. Gotthardt, Philos. Mag. A78 (1998) 327.
[2] J. Khalil-Allafi, A. Dlouhy, G. Eggeler, Acta Mater. 50 (2002) 4255.
[3] K. Gall, H. Sehitoglu, Y.I. Chumlyakov, I.V. Kireeva, H.J. Maier, J. Eng. Mater.-T. ASME 121 (1999) 19.
[4] R. Santamarta, D. Schryvers, Mater. Sci. Eng. A 378 (2004) 143.
[5] R. Santamarta, D. Schryvers, Mater. Trans. 44 (2003) 1760.
[6] Y. Nishida, C.M. Wayman, T. Honma, Metal. Trans. A17 (1986) 1505.
[7] W. Tirry, D. Schryvers, Mater. Sci. Eng. A 378 (2004) 157.
[8] T. Tadaki, Y. Nakata, K. Shimizu, K. Otsuka, T. Jpn. I. Met. 27 (1986) 731.
[9] C. Somsen, Mikrostrukturelle Untersuchungen an Ni-reichen Ni-Ti Formgedächtnislegierungen, Shaker Verlag, Aachen, 2002, p. 14.
[10] A. Rosenauer, G. Gerthsen, Adv. Imag. Elect. Phys. 107 (1999) 121.
[11] D. James, G. Zanzotto (personal communication).